J. Phys. B: At. Mol. Opt. Phys. **33** (2000) 615–635. Printed in the UK PII: S0953-4075(00)05836-3

Electron and positron scattering from halogenated methanes: a comparison of elastic cross sections

R Curik†‡ F A Gianturco†§ and N Sanna‡

† Department of Chemistry, the University of Rome, Città Universitaria, 00185 Rome, Italy
‡ Supercomputing Center for University and Research, CASPUR, Piazzale A Moro 5, 00185 Rome, Italy

E-mail: fagiant@caspur.it

Received 8 June 1999, in final form 2 November 1999

Abstract. This paper discusses the use of quantum scattering methods for the evaluation of the elastic (rotationally summed) integral and differential cross sections produced in collisions at low energies ($E_{\rm coll} \leqslant 20$ eV) of electrons and positrons with polyatomic gaseous targets. The calculations use close-coupled equations and a parameter-free model of electron and positron interactions with the molecules in a single-collision situation. Comparison with existing experiments on the collision processes with the two projectiles helps us to know more detail about the features of the forces in play during the scattering events. Computed results are also found to be in good accord with experiments.

1. Introduction

The existence of the positron, the antiparticle corresponding to the electron, has been known for quite a long time (see, e.g., Massey 1932) and therefore the development of experiments with positrons, together with several attempts at their theoretical interpretation have played an important role in our understanding of fundamental aspects of the structure of matter in its various states of aggregation (Humbertson and Armour 1988, Griffith 1979).

In the area of atomic and molecular physics the new presence of the positron made it possible to devise a whole new range of scattering experiments which would be complementary to those that could be carried out using electrons as probing projectiles. The simple fact that the charges of the two probes carry a different sign already has several important consequences. The positron is further distinguishable from the bound target electrons and therefore exchange effects with the incident particle are absent. In contrast to the electron, the positron is attracted by the target electrons and repelled by the molecular nuclei. Thus, the probability of the incident particle being close to a target electron is much greater for positron scattering while, at the same time, the electron projectile penetrates more deeply inside the molecular volume due to the strong nuclear attraction terms which exist in its case. Furthermore, the outcomes of inelastic scattering processes, even if one limits the analysis to low collision energies, for the case of positron projectiles provide a new variety of channels which are missing in the case of electron scattering, e.g. Positronium (Ps) formation and positron annihilation. Conversely, a typical feature of electron scattering from molecular targets at low collision energies, i.e.

§ Author to whom correspondence should be addressed.

0953-4075/00/040615+21$30.00

the presence of trapping shape resonances without target excitation, is largely missing when positron scattering is examined.

The above considerations therefore make it rather useful to compare the behaviour between electrons and positrons as projectiles when multielectron polyatomic ambient gases are studied. The latter types of target, in fact, provide a large variety of electronic properties in their ground states and consequently are expected to exhibit a similar variety in the behaviour of their scattering attributes when they are probed with the above two particles as projectiles.

In the present study we will be considering a computational approach to the evaluation of elastic scattering cross sections (integral and differential) for both electrons and positrons as projectiles and using two polyatomic, many-electron targets as examples: the CF_4 and CCl_4 molecules. The following section briefly summarizes the present formulation of the scattering equations and discusses our selection of the interaction potentials. Section 3 reports the results for electron scattering and compares them with the existing experiments, while section 4 gives similar calculations and comparisons for the case of positron scattering processes. Section 5 summarizes our present conclusions and the possible extensions of the present methodology to larger, and more complex ambient gases.

2. Scattering equations and interaction forces

2.1. The single-centre expansion dynamics

Resonant and non-resonant low-energy scattering of positrons and electrons from polyatomic targets can be studied theoretically (and computationally) at various levels of sophistication for the description of: (a) the electronuclear structure of the target molecule, (b) the interaction forces between the bound particles and the impinging electron and (c) the dynamical formulation of the quantum scattering equations (Gianturco and Jain 1986).

Within an *ab initio*, parameter-free approach one could start with the target nuclei being kept fixed at their equilibrium geometry and their motion during the scattering process could then be decoupled from the other variables. The simplifying scheme goes under the familiar name of the fixed-nuclei (FN) approximation (Itikawa 1997) and it strongly reduces the dimensionality of the coupled equations for the dynamics. Furthermore, the target N electrons bound in a specific molecular electronic state (which, for the present purpose, is taken as unchanged during the scattering) can be described within the near-Hartree–Fock, self-consistent field (SCF) approximation by using the single-determinant (SD) description of N occupied molecular orbitals (MOs). In our implementation of the scattering equations the occupied MOs of the targets are again expanded on a set of symmetry-adapted angular functions with their corresponding radial coefficients represented on a numerical grid (Gianturco *et al* 1994b). In this approach, any arbitrary three-dimensional function describing a given electron, either one of the N bound electrons or the scattering electron, is expanded around a single-centre (SCE) usually taken to be the centre of mass of the global $(N + 1)$-electron molecular structure

$$F^{p\mu}(r, \hat{\boldsymbol{r}}|\boldsymbol{R}) = \sum_{l,h} r^{-1} f_{lh}^{p\mu}(r|\boldsymbol{R}) X_{lh}^{p\mu}(\hat{\boldsymbol{r}}). \tag{1}$$

The above SCE representation refers here to the μth element of the pth irreducible representation (IR) of the point group of the molecule at the nuclear geometry $\boldsymbol{R}$. The angular functions $X_{lh}^{p\mu}(\hat{\boldsymbol{r}})$ are symmetry-adapted angular functions given by a proper combination of

spherical harmonics $Y_{lm}(\hat{\boldsymbol{r}})$

$$X_{lh}^{p\mu}(\hat{\boldsymbol{r}}) = \sum_m b_{lmh}^{p\mu} Y_{lm}(\hat{\boldsymbol{r}}). \tag{2}$$

The details about the computation of $b_{lmh}^{p\mu}$ have been given by us before and will not be repeated here (Gianturco *et al* 1994b).

Once all the bound and continuum wavefunctions have been expanded using (1), then the quantum scattering equations will give us a way of evaluating the unknown radial coefficients of (1) for the $(N+1)$th continuum electron, scattered off the N-electron target, by using the SCE radial quantities for the occupied target MOs. For electron scattering, for instance, we additionally have to consider exchange terms as

$$\left[\frac{\mathrm{d}^2}{\mathrm{d}r^2} - \frac{l(l+1)}{r^2} + 2(E-\epsilon_\alpha)\right] f_{lh}^{p\mu,\alpha}(r|\boldsymbol{R}) = 2\sum_{l'h'\beta}\int \mathrm{d}r'\, V_{lh,l'h'}^{p\mu,\alpha\beta}(r,r'|\boldsymbol{R})\, f_{l'h'}^{p\mu,\beta}(r'|\boldsymbol{R}) \tag{3}$$

where E is the collision energy $E = k^2/2$ and ϵ_α is the electronic eigenvalue for the αth asymptotic state. The $p\mu$ indices employed on the right-hand side of equation (3) now label the specific μth component of the pth IR that belongs to the αth electronic target state (initial state) coupled with the infinity of excited state IRs labelled collectively by β. The coupled partial integro-differential equations (IDEs) (3) contain the kernel of the integral operator V which is thus a sum of diagonal and non-diagonal terms that in principle can fully describe the electron–molecule interaction during the collision process. When one uses the near-HF wavefunction from an SD-SCF calculation to represent the bound target electrons and further truncates the sum on the right-hand side of equation (3) to one state α only, one obtains the exact-static-exchange (ESE) representation of the electron–molecule interaction for the chosen electronic target state (usually the ground state) at the nuclear geometry $\boldsymbol{R}$. Introducing the assumption of having only a local e^-–molecule interaction one can further simplify equation (3)

$$\left[\frac{\mathrm{d}^2}{\mathrm{d}r^2} - \frac{l_i(l_i+1)}{r^2} + k^2\right] f_{ij}^{p\mu}(r|\boldsymbol{R}) = \sum_n V_{in}^{p\mu}(r|\boldsymbol{R})\, f_{nj}^{p\mu}(r|\boldsymbol{R}) \tag{4}$$

where the indices i, j or n represent the 'angular channel' $|lh\rangle$ and the potential coupling elements are given as

$$V_{in}^{p\mu}(r|\boldsymbol{R}) = \langle X_i^{p\mu}(\hat{\boldsymbol{r}})|V(\boldsymbol{r}|\boldsymbol{R})|X_n^{p\mu}(\hat{\boldsymbol{r}})\rangle = \int \mathrm{d}\hat{\boldsymbol{r}}\, X_i^{p\mu}(\hat{\boldsymbol{r}})\, V(\boldsymbol{r}|\boldsymbol{R})\, X_n^{p\mu}(\hat{\boldsymbol{r}}). \tag{5}$$

The standard Green's function technique allows us to rewrite the previous differential equations in an integral form

$$f_{ij}^{p\mu}(r|\boldsymbol{R}) = \delta_{ij}\, j_{l_i}(kr) + \sum_n \int_0^r \mathrm{d}r'\, g_{l_i}(r,r')\, V_{in}(r'|\boldsymbol{R})\, f_{nj}^{p\mu}(r'|\boldsymbol{R}). \tag{6}$$

The integral on the right-hand side of equation (6) terminates at $r' = r$ (integral equations with this property are called Volterra equations), because the regular Green's function $g_{l_i}(r,r')$ is used

$$g_l(r,r') = \frac{1}{k}\left[\hat{j}_l(kr)\,\hat{n}_l(kr') - \hat{n}_l(kr)\,\hat{j}_l(kr')\right] \tag{7}$$

where $\hat{j}_l(kr)$ and $\hat{n}_l(kr)$ are Riccati–Bessel and Riccati–Neumann functions. The numerical implementation and stabilization corrections for integral equations (6) have been discussed

for diatomics before (Sams and Kouri 1969, Rescigno and Orel 1981, 1982) and the obvious generalization for polyatomic systems will not be repeated here.

For a target which has a closed-shell electronic structure, as in the present examples, with $n_{\rm occ}$ doubly occupied orbitals φ_i, the potential can be written, for the case of electron scattering, as first given by its static + exchange contributions

$$V_{\rm SE}(\boldsymbol{r}) = \sum_{\alpha=1}^{M} \frac{Z_\alpha}{|\boldsymbol{r} - \boldsymbol{R}_\alpha|} + \sum_{i=1} n_{\rm occ}(2\hat{J}_i - \hat{K}_i) \tag{8}$$

where $\hat{J}_i$ and $\hat{K}_i$ are the usual local static potential and the non-local exchange potential operators, respectively. The index α labels one of the M nuclei located at the coordinate $\boldsymbol{R}_\alpha$ in the centre-of-mass, molecular frame of reference (MF). Electron–molecule scattering cross sections (integral and differential) which are computed using the $V_{\rm SE}$ potential sometimes show a modicum of agreement with experimental data of elastic scattering provided they are at about 10–15 eV and away from resonant features (see, e.g., Huo and Gianturco 1995), while they turn out not to be realistic enough when the simple static potential, $V_{\rm st}$ (no exchange term) is employed for positron scattering (Mc Alinden *et al* 1994). The reason for the limited validity of equation (8), or of its counterpart for positron scattering, lies in its lack of description of the target response, i.e. of the effects of long-range polarization of the bound electrons by the charged projectile and of the short-range dynamical correlation between the latter and the molecular electrons which occur during the scattering.

At higher collision energies this is reflected in the fact that no electronically inelastic processes can be treated at the SE level of interaction. At the lower energy, of more direct interest in the present study, the lack of inclusion of the target response leads to the neglect of important polarization effects which then causes the wrong energy behaviour and magnitude of the cross sections and, furthermore, can significantly alter the energy location and the obtained width of the resonances occurring at those energies. This difficulty could be avoided by the inclusion of additional target states in the expansion of the target wavefunction. Such an approach, however, can significantly increase the computational complexity of solving the scattering equations and is not equally well defined in its implementation for electrons and positrons (see, e.g., Mc Alinden *et al* 1994). We will therefore discuss below the different computational options we have used for electrons and positrons as projectiles.

2.2. The electron–molecule model interaction

In the present treatment of electron scattering from multielectron, polyatomic targets we have also employed a simpler form of exchange interaction in order to more rapidly implement the comparative study of scattering attributes between electrons and positrons as projectiles. Thus, we replaced the non-local contributions in equation (3) with two different, approximate models: (a) with an energy-dependent, local exchange potential suggested long ago from a free-electron-gas (HFEGE) model for the continuum–bound electron exchange (Hara 1967). Since this simpler model treatment has also been discussed by us in our earlier work (Gianturco and Jain 1986) we will not repeat its detailed description here. Suffice it to say that, in spite of its very straightforward implementation, the HFEGE model is still frequently used with surprising success for treating polyatomic targets (see, e.g., Itikawa 1997). In the following the local form of the model exchange will be called the HFEGE exchange interaction. Another model used here (b) semiclassical exchange (SMCE) treats the bound–continuum exchange interaction a bit more realistically then the HGEFE model in the sense that the local momentum

of the bound electrons can be disregarded with respect to that of the impinging electron thereby leading to the neglecting of the gradients of molecular orbitals with respect to the gradient of the wavefunction for the projectile (Riley and Truhlar 1975, Gianturco and Scialla 1987a–c). The details of its derivation have been given extensively in the above references and therefore they will not be repeated here.

Further, to include in the electron–molecule potential the long-range polarization terms and the short-range dynamical correlation effects discussed before, we have additionally implemented the inclusion of a local, energy-independent model potential, $V_{\rm ecp}(\boldsymbol{r})$ for electron collisions which was already discussed previously in our work (Gianturco *et al* 1987). Briefly, the $V_{\rm ecp}$ model potential contains a short-range correlation contribution, $V_{\rm corr}$, which is smoothly connected to a long-range polarization contribution, $V_{\rm pol}$, both terms being specific for electron projectiles. The short-range term is obtained by defining an average dynamic correlation energy of a single electron within the formalism of the Kohn and Sham variational orbitals representing the bound electrons. The functional derivative of such a quantity with respect to the SCF N-electron density of the molecular target provides a density-functional description of the required short-range correlation term (for a general discussion of DFT methods see Parr and Yang (1989)). The long-range part of $V_{\rm ecp}$ is obtained by first constructing a model polarization potential, $V_{\rm pol}$, which asymptotically agrees with the potential obtained from the static dipole polarizability of the target in its ground electronic state. This corresponds to including the dipole term in the second-order perturbation expansion of the polarization potential. One can construct such a model either by choosing a single 'polarization' centre or by partitioning the total static polarizability between different centres: in the present case the former option has turned out to be fairly realistic, as we shall discuss further below.

Since in the general case, the long-range contribution, $V_{\rm pol}$, does not exactly match the short-range correlation, $V_{\rm corr}$, at any given value of r, one needs an appropriate $r_{\rm match}$ by first performing a single-centre expansion of both contributions and by then finding where the two radial coefficients for $l = 0$ first intersect. This has, in fact, been what we found in many cases to be the more effective choice in terms of the global smoothness of the total potential (Gianturco *et al* 1994a). Hence, one writes down the full potential as

$$V_{\rm ecp}(\boldsymbol{r}_{\rm e}) = \begin{cases} V_{\rm corr}(\boldsymbol{r}_{\rm e}) & r_{\rm e} \leqslant r_{\rm match} \\ V_{\rm pol}(\boldsymbol{r}_{\rm e}) + \displaystyle\sum_{lm} C_{lm} r^{-\lambda} Y_{lm}(\hat{\boldsymbol{r}}_{\rm e}) & r_{\rm e} > r_{\rm match} \end{cases} \tag{9}$$

where the use of $\boldsymbol{r}_{\rm e}$ here underlines that the variable in equations (3) and (4) specifically refers to the electron projectile. The C_{lm} coefficients have been determined to make the potential continuous at $r_{\rm match}$ and the exponent λ is a function of l such that: $\lambda(l) = 6, 5, 6$ for $l = 0, 1, 2$ and $\lambda(l) = l + 2$ for $l \geqslant 3$. The matching functions are chosen so that each term added to $V_{\rm pol}$ after $r_{\rm match}$ has the same functional form of the first term neglected in the perturbation expansion of $V_{\rm pol}$. The new, full interaction now corresponds to carrying out the scattering equation using the static-exchange correlation–polarization (SEP) level of interaction. We shall see in the following discussion of our results in comparison with experimental findings that the $V_{\rm SECP}$ model interaction is indeed capable of providing a very realistic description of, and nearly quantitative agreement with, the experimental values of the elastic (rotationally summed) integral cross sections for CF_4 and CCl_4 polyatomic targets.

2.3. The positron–molecule potential

If we leave out for the moment specific considerations of inelastic precesses, except those involving molecular rotations or vibrations (which, however, we will disregard just now in our calculations because of a lack of reliable data in the case of positron–molecule scattering) we could represent the interaction between the incident particle and the target by an effective one-body potential V_{sp} made up of two main terms

$$V_{sp}(\boldsymbol{r}_p) = V_{st}(\boldsymbol{r}_p) + V_{pol}(\boldsymbol{r}_p). \tag{10}$$

The subscript in $\boldsymbol{r}_p$ now underscores the presence of a positron projectile. As mentioned earlier, the last contribution is the correction term which must be added to V_{st} to take into account the effects of the distortion of the molecular target charge distribution by the incident charged particle. It is easy to show, using the well known properties of spherically symmetric electronic charge distributions and of point nuclear and electronic charges interacting through an inverse-square Coulombic force (Dalgarno and Lewis 1956), that V_{st} must be attractive for electron scattering by a neutral atomic target and that it simply changes sign in the case of positron scattering. This contribution is therefore largely repulsive for the latter projectile. The situation is really more complicated for a molecular target as the overall potential is no longer spherical. However, the above result still holds when the nature of V_{st} over all incident positron–molecule separation is examined (Armour 1989).

The correction term V_{pol}, however, is made up of terms which are of second- and higher-order terms in the Coulombic interaction between the positron and the molecule. If one considers for the moment the second-order term only, it is well known that for an atom or molecule in its ground electronic state such a term is negative irrespective of the sign of the perturbing interaction (see, e.g., Gianturco *et al* 1994a), although the higher-order terms carry a sign controlled by that of the charged projectile (Buckingham 1967). Furthermore, the magnitude of the perturbation increases as the incident particle approaches the molecule. It is important to realize, however, that the molecular charge distribution is being perturbed by a moving particle and not by a fixed charge. One consequence is that V_{pol} has its largest effect at the lowest collision energies and steadily decreases as the energy increases, thereby becoming dominated by the V_{st} contributions: in the positron scattering, as opposed to the electron collisions, at the lower energies V_{st} and V_{pol} tend to oppose each other and therefore the actual values of the molecular second- and higher-order polarizabilities play a crucial role in controlling the cross section behaviour.

One of the important differences between positron and electron scattering lies in the fact that each bound electron and the impinging positron attract each other and therefore accurate representations of V_{pol} in the short-range regions require the knowledge of the total wavefunction when the positron is in the vicinity of the target electrons and where the pseudo-one-body potential of equation (10) is no longer valid (Armour and Baker 1987).

In the present study we therefore decided to describe that short-range region of interaction, V_{corr}, for the case of a continuum positron and N bound electrons, by modifying the V_{ecp} potential using a correlation–polarization form specifically suited to positron projectiles

$$V_{ecp} \Rightarrow V_{p-mol}(\boldsymbol{r}_p) = V_{st}(\boldsymbol{r}_p) + V_{corr}(\boldsymbol{r}_p) + V_{pol}(\boldsymbol{r}_p) \tag{11}$$

where the V_{st} is simply the same as that of equation (8), but with its signs changed and without the exchange contributions. The long-range part of the V_{pol} was described by the spherical component of the dipole polarizability term (Jain and Gianturco 1991) which was then added to the multipolar terms of equation (9) obtained, as discussed before, by numerical matching

but now at a different $r_{\rm match}$ value. The crucial part of the above potential for describing short-range features of the positron–electron interaction resides in the choice of the correlation term, $V_{\rm corr}$. One choice could be to simply employ for the positron the same $V_{\rm ecp}$ potential as in equation (9). Another option is to take into account the different physics of positron–electron correlation by modelling it through the positron correlation in the electron gas (Boronski and Nieminen 1986). In the latter instance, when the incoming positron enters the target electronic charge cloud one could assume that the positron 'impurity' is quickly localized within the surrounding electrons of a given density $\rho(\boldsymbol{r}_{\rm e})$ and can be described through the dynamics of the new particle in a positron–electron plasma (Arponen and Pajanne 1979). Hence, as in the case of equation (9), one can write down a similar relation to obtain the last two terms of equation (11),

$$\begin{aligned} V_{\rm pcp}(\boldsymbol{r}_{\rm p}) &= V_{\rm corr}(\boldsymbol{r}_{\rm p}) \qquad r_{\rm p} \leqslant r_{\rm match} \\ V_{\rm pcp}(\boldsymbol{r}_{\rm p}) &= V_{\rm pol}(\boldsymbol{r}_{\rm p}) \qquad r_{\rm p} > r_{\rm match}. \end{aligned} \tag{12}$$

The details of $V_{\rm pcp}(\boldsymbol{r}_{\rm p})$ have been given several times before and will not be repeated here (Jain and Gianturco 1991, Gianturco *et al* 1993).

Another modelling of the above $V_{\rm pcp}$ could be obtained by first generating numerically, through repeated self-consistent-field calculations for the target bound molecular orbitals the perturbation caused by a positive point charge kept fixed in space over a sufficient range of (r, ϑ, φ) values which would allow the generation of different $V_{\rm st}$ points with each new set of perturbed MOs. They would thus provide a new, perturbed static interaction, $V_{\rm st}^{\rm pol}(\boldsymbol{r}_{\rm p})$. An estimate of the short-range behaviour of the polarizing effect of a positive point charge could then be obtained on the grid of (r, ϑ, φ) by writing

$$V_{\rm pcp}(\boldsymbol{r}_{\rm p}) \Rightarrow V_{\rm pscf}(\boldsymbol{r}_{\rm p}) = V_{\rm st}^{\rm pol}(\boldsymbol{r}_{\rm p}) - V_{\rm st}^{p}(\boldsymbol{r}_{\rm p}) \qquad r_{\rm p} \leqslant r_{\rm match} \tag{13}$$

while the long-range polarization could be obtained via the usual matching described before. In summary, we have tested three different modelling options for the short-range correlation effects between the positron projectile and the bound electrons of the target. (a) The use of the same $V_{\rm ecp}$ model discussed before for the electron projectiles; (b) a different formulation of the latter which specifically deals with positrons, the $V_{\rm pcp}$ of above and (c) the short-range correlation modelled via a positive point charge, the $V_{\rm pscf}$ of equation (13). The idea here is to try to develop some systematic assessment of possible models of this important interaction term when treating low-energy positron collisions with multielectron polyatomic targets.

Just to give a pictorial idea of their shapes, we present in figure 1 the relative behaviour of the above model potentials for the CF_4 molecule (top panel) and the CCl_4 molecule (lower panel). We can easily see the following:

(a) in both cases the $V_{\rm ecp}$ gives the weakest correlation potential with the bound electronic charge densities and extends over a rather large region of space before matching the $V_{\rm pol}$ interaction ($r_{\rm match}$ around 5 a_0);
(b) the positron–electron correlation, $V_{\rm pcp}$, is instead much stronger in the inner region and shows a different matching radius depending on the molecular target: about 2 a_0 for CF_4 and about 2.8 a_0 for the larger CCl_4 system;
(c) the perturbation potential $V_{\rm pscf}$, on the other hand, shows great changes between CF_4 and CCl_4: the larger number of outer electrons for the latter molecule, in fact, produces a stronger polarization effect in the inner region and extends it out to more than 3 a_0. The more compact CF_4 target shows instead a very short-range behaviour similar to $V_{\rm pcp}$ but remains weaker than the latter in the region before the $r_{\rm match}$ value around 2.2 a_0.

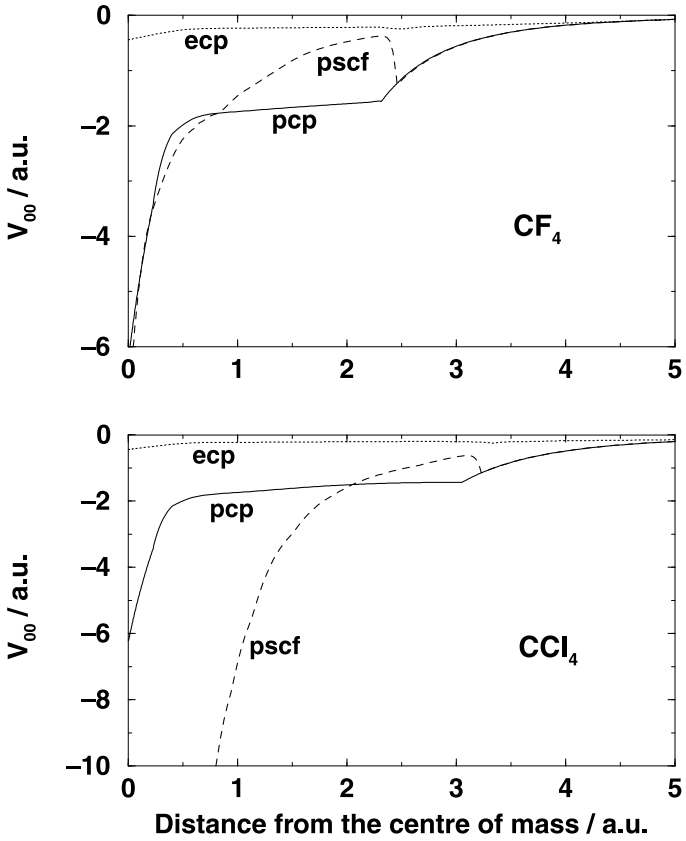

Figure 1. Computed spherical components of model potentials for correlation–polarization forces. Upper panel, results for CF_4; lower panel, results for CCl_4. The full curves refer to the V_{pcp} potential described in the main text. The broken curves show the V_{pscf} potential calculations, while the dotted curves indicate the V_{ecp} potentials.

We therefore expect that such marked differences will affect the low-energy behaviour of the elastic cross sections. We shall show the latter quantities in the following sections.

3. Electron scattering results

We carried out calculations for CF_4 and CCl_4 polyatomic targets which were kept at their equilibrium geometries and electronic ground states. The carbon–halogen distances were 1.320 Å for CF_4 and 1.766 Å for CCl_4 (Weast and Salby 1966). The FN approximation was employed throughout the present study and single determinant configurations were used. The multicentre expansion over Gaussian orbitals was in both cases at the D95* level (80 basis functions for CF_4 and 112 for CCl_4, respectively) using the Gaussian 94 suite of codes (Pritsch *et al* 1995). The corresponding near-HF, SCF energies were: -435.7654 au for CF_4 and -1875.7202 au for CCl_4. For the long-range V_{pol} we employed the experimental dipole polarizabilities of 19.6 au for CF_4 and 70.5 au for CCl_4 (Miller 1990).

When constructing the static potential, V_{st}, the single-centre expansion of the nuclear singularities for the electron scattering included values of angular momenta up to 80 for CF_4 and up to 100 for CCl_4; likewise, the electronic densities included the same number of terms

for each molecule as the nuclear part. Finally, the partial-wave expansions for the continuum electron went up to $l = 40$ for CF_4 and $l = 50$ for CCl_4. This means that the A_1 symmetry involved 81 coupled equations for the former target and 121 for the latter molecule. The T_1 and T_2 symmetries, therefore, included 200 and 220 close-coupled (CC) equations for CF_4 and 312 and 338 equations for CCl_4. The remaining irreducible representations, A_2 and E, included 60 and 140 CC equations for CF_4 and 96 and 217 equations for CCl_4. The radial integrations used to solve the corresponding integral equations (6) extended out to $r_{max} = 34$ au.

The carbon tetraflouride molecular gas is of considerable importance in a wide variety of technological applications. Because it shows little reactivity in its ground electronic state and has no bound excited electronic states, it is frequently employed as a feed gas in the plasma etching of semiconductors. One therefore needs to understand in a far more detailed fashion the complex chemistry and the competitive kinetics which take place in a plasma environment containing this gas and other chemical species such as SiH_4, SiO_2, etc. A recent review (Christophorou *et al* 1996) surveys all theoretical and experimental work on e^-–CF_4 collisions and interactions to that date. The latest calculations on electron–CF_4 have been carried out by Isaacs *et al* (1998) using the complex Kohn method and suggested the existence of a Ramsauer–Townsend (RT) minimum in that system. In general terms, the low-energy cross sections which are of interest in the present comparison between electron and positron scattering behaviour are characterized by a broad shape resonance around 9 eV and a smooth decrease below 6 eV. Both features are of interest for testing the reliability of the model

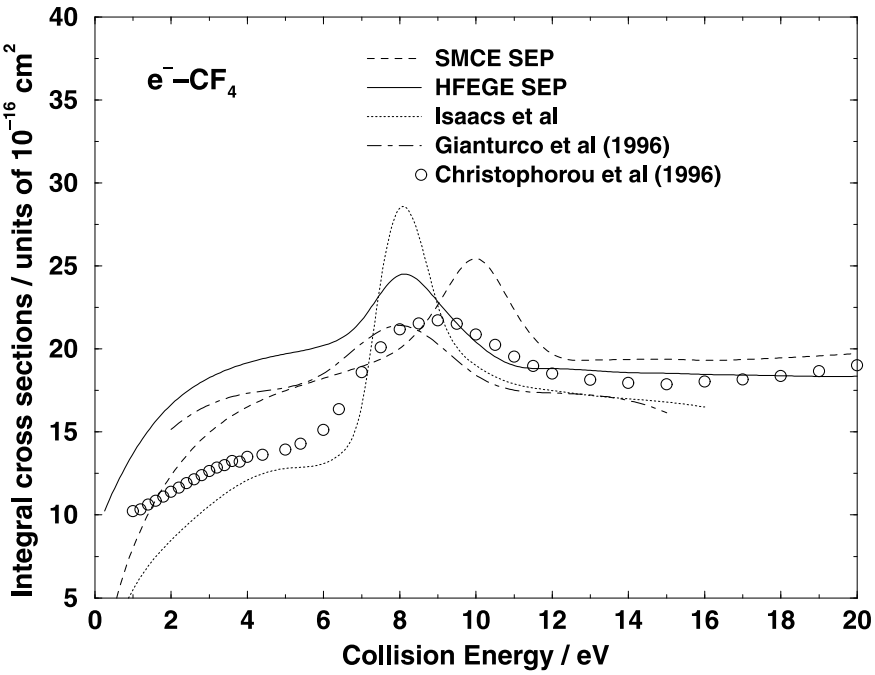

Figure 2. Computed and measured integral cross sections for electron–CF_4 scattering. Open circles, recommended experimental cross sections from Christophorou *et al* (1996). Full curve, present calculations of elastic integral cross sections for the continuum electron and the HFEGE exchange potential; broken curve, present calculations using the semiclassical exchange; dotted curve, calculations of Isaacs *et al* (1998); chain curve, previous results with exact exchange (Gianturco *et al* 1996).

Table 1. Computed partial and total integral cross sections (units of $Å^2$) of the present work for the CF_4 and CCl_4 molecular targets (SMCE calculations) over a selected range of collision energies (eV).

	CF_4			CCl_4			
E (eV)	σ_{A_1}	σ_{T_2}	σ_{tot}	σ_{A_1}	σ_E	σ_{T_2}	σ_{tot}
0.5	0.70	0.36	4.39	37.63	0.35	0.55	40.16
1.0	7.19	0.19	8.02	44.92	0.34	2.99	54.96
2.0	10.04	0.66	12.38	24.00	0.12	8.49	50.20
3.0	10.21	1.46	14.96	12.70	0.23	15.69	60.69
4.0	9.49	2.24	16.51	6.47	0.66	20.67	70.43
5.0	8.53	2.89	17.49	3.53	1.34	16.93	58.10
6.0	7.59	3.44	18.23	2.50	2.40	16.03	57.33
7.0	6.74	3.93	18.95	2.46	4.21	15.70	61.17
8.0	6.01	4.49	20.04	2.87	6.53	15.00	65.91
9.0	5.41	5.50	22.67	3.41	7.37	14.19	67.96
10.0	4.93	6.51	25.45	3.91	6.83	13.39	67.52
12.0	4.60	4.52	19.70	4.54	6.27	11.49	65.29
14.0	4.49	4.24	19.36	4.67	6.54	9.79	61.94
16.0	4.05	4.14	19.31	4.48	6.43	8.70	58.61
18.0	3.80	4.02	19.46	4.16	6.04	8.12	56.54
20.0	3.65	3.88	19.72	3.85	5.66	7.96	54.86

potentials employed in the present work. We report in figure 2 the behaviour of our calculated integral elastic cross sections in the energy range between 1.0 and 20 eV, together with the recommended experimental values for the total cross sections (Christophorou *et al* 1996) over the same range of energies. The actual numerical values of the present cross sections are reported, for selected energies, in table 1. We also show in the same figure the latest complex Kohn calculations (Isaacs *et al* 1998) and our previous results with exact exchange (Gianturco *et al* 1996). Considering the convergence in the partial-wave expansion we see clearly that, in the case of a molecule with the presence of substantial nuclear and electronic charges located off the expansion centre, the convergence requires the inclusion of many angular momentum values. The maximum of $l = 40$ corresponds to converged results for the two sets of cross sections computed here: the one which used the HFEGE model exchange (full curve) and the one using the semiclassical exchange model also proposed by us in our earlier work (Gianturco and Scialla 1987a–c) and briefly outlined in the previous section (dotted curve). We see from the results in the figure that it is essential for reproducing the marked drop of the cross sections below 6 eV, as reported by the experiments, to employ the more sophisticated SMCE form of exchange potentials which we had tested on CH_4 targets long ago. The shape and position of the resonance maximum is also given rather well by our calculations which locate it between 8 and 10 eV, not far from the 9 eV of the experiments.

The low-energy behaviour of the cross section is known to be crucially dependent, for non-polar molecules, on the polarization and correlation terms of the interaction. Given the present modelling of V_{ecp}, therefore, it is not surprising to see that our model calculations yield only semiquantitative agreement with the measured data below the resonant maximum. On the whole, however, we feel that the present treatment of the interaction forces can, with limited computational effort, provide a fairly realistic description of the electron scattering from a multielectron polyatomic target such as CF_4 and does not depart too much from experiments.

The CCl_4 target also belongs to the same class of halogenated hydrocarbons which have

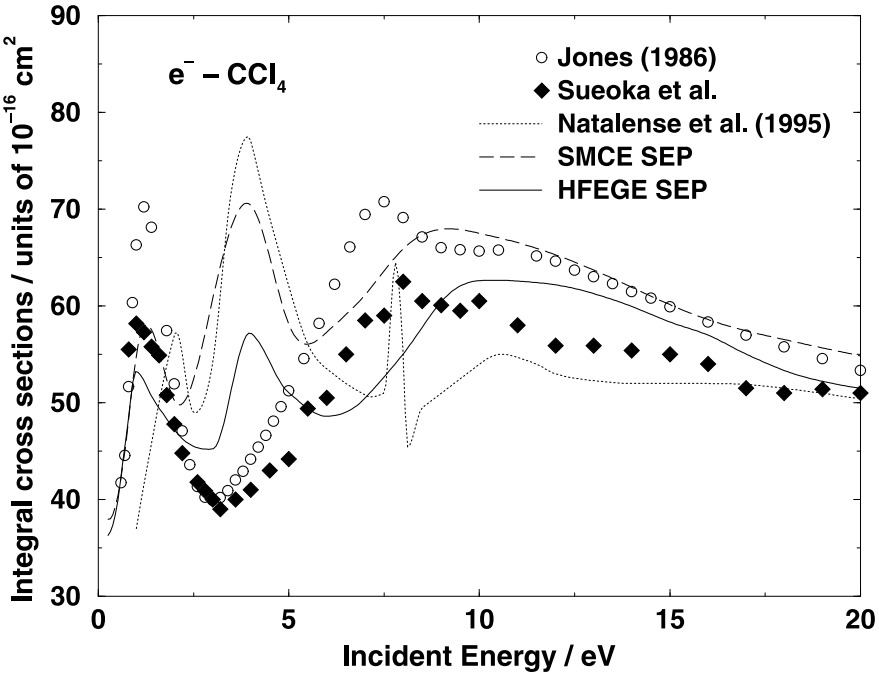

Figure 3. Computed and measured cross sections for electron–CCl_4 scattering. Experiments: open circles, Jones (1986); full diamonds, Sueoka *et al* (1999). Calculations: dotted curve, Natalense *et al* (1995); full curve, present results with $l_{max} = 50$ and the HFEGE exchange model; broken curve, present results with the semiclassical exchange model.

shown great importance for the implementation of plasma etching of semiconductors. On the other hand, because of its larger number of electrons (80 bound MOs in its ground electronic state), and because of the larger Z values of the off-centre nuclear charges it also constitutes a greater challenge for the computations: therefore, very few attempts exist at evaluating its scattering attributes. The most recent of them is the calculation of Natalense *et al* (1995) who employed a norm-conserving pseudopotential method within the Schwinger multichannel method (SMC) (Bettega *et al* 1993). Only the SE potential was used in their work. The experimental data for the total cross sections are in some disagreement with each other and come from two sets of measurements: those from Jones (1986) and those from Sueoka *et al* (1998). In figure 3 we show a comparison of the present calculations with the earlier theoretical results (dotted curve) and with the two sets of experiments (open circles and full diamonds). The actual numerical values of the present cross sections are shown, for selected energies, in table 1. Our results show the behaviour of the elastic cross section using the model SEP interactions and converged results with a maximum $l = 50$ for the continuum electron. The two different exchange models were employed: the HFEGE local exchange (full curve) and the SMCE (broken curve).

The following comments could be readily made from the above comparison.

(a) The experiments show a broad maximum around 8 eV, as in the case of CF_4, but also, at lower energy, a narrower peak around 1 eV with, at its maximum, an intensity as large as that of the higher-energy, broader resonance. They also indicate the presence of a drastic

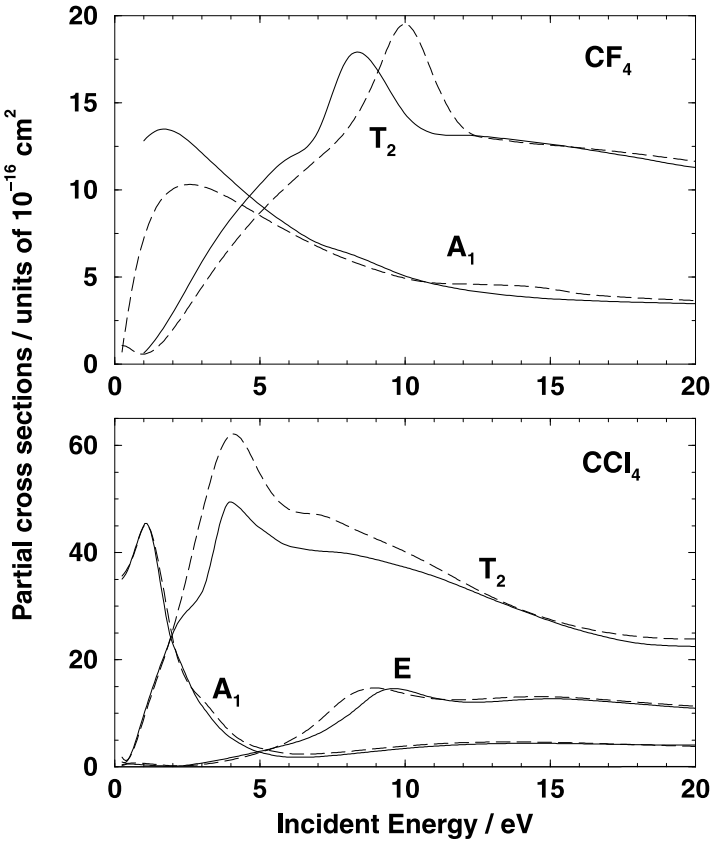

Figure 4. Computed partial cross sections for each of the contributing irreducible representations. Upper panel, results for CF_4; lower panel for CCl_4. Full curves, HFEGE exchange; broken curves, semiclassical exchange.

drop of intensity at very low energies.

(b) The pseudopotential calculations (Natalense *et al* 1995) give the two peaks shifted to higher energies (no polarization effects were included in their treatment).

(c) The present calculations describe the broad maximum at higher energies, with both model results fairly close to the experimental behaviour above about 8 eV. The low-energy maximum of T_2 symmetry, however, appears shifted to higher energies by all calculations while the second, lower maximum of A_1 symmetry is given by the present and by the earlier calculations (Natalense *et al* 1995) although it is not visible in the experiments because of the stronger T_2 resonance. Here again both the calculations and the experiments suggest the presence of a low-energy RT-type minimum structure.

In order to better understand the features of both computed and measured cross sections, we report in figure 4 the behaviour of the partial contributions to the total elastic quantity from all the irreducible representations (IR) which yielded non-negligible values. Only the results from the converged expansion are shown in the figure. Once more the full curves refer to the HFEGE model exchange and the broken curves to the SMCE calculations (Gianturco and Scialla 1987a).

In the previous analysis of the various symmetry components of the total elastic cross

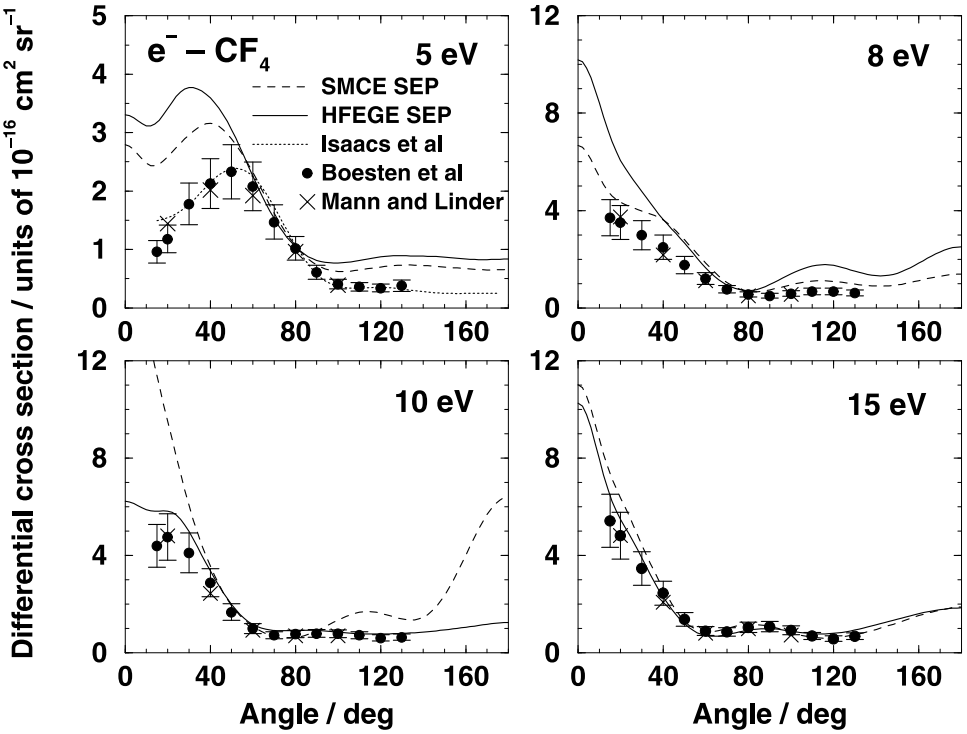

Figure 5. Computed and measured elastic differential cross sections (DCS) for electron scattering from CF_4 at four different values of collision energy. Full curve, HFEGE exchange. Broken curve, semiclassical exchange. Full circles, experimental data of Boesten *et al* (1992). Crosses, experimental data of Mann and Linder (1991). The complex Kohn calculations of Isaacs *et al* (1998) are given by the dotted curves.

sections for the electron CF_4 scattering (see, e.g., Gianturco *et al* 1996), the resonance around 9 eV in the experiments was attributed to electron trapping in the T_2 symmetry, i.e. involving antibonding orbitals of the fluorine atoms, while the low-energy behaviour has been found to be dominated by the A_1 symmetry component which could give rise to a Ramsauer–Townsend minimum down to 0.1–0.2 eV (Isaacs *et al* 1998). The broad shoulder seen by the experiments around 3.6 eV (Jones 1986) is shown by our calculations to be due to the opposite energy dependence of the two symmetry components and it tends to become reduced in magnitude as the A_1 component turns down at lower energies to produce the RT feature: it is, however, shifted to about 4 eV by the complex Kohn calculations (Isaacs *et al* 1998). To ascertain whether the experimental broadening should be attributed to inelastic effects, and therefore is not well given by only elastic FN calculations, would require direct coupling with at least vibrationally inelastic channels, a procedure which we have not attempted in the present work.

The model calculations results of figure 4 do manage to show, however, that only one resonant feature is present below 20 eV for the CF_4 target, in agreement with the experimental suggestions. They also indicate that the marked drop of the total elastic cross sections below 6 eV could produce a Ramsauer–Townsend minimum very close to the zero-energy threshold and that its appearance requires a delicate balance between exchange interactions and the long-range polarization contributions.

In the case of CCl_4 molecular gas the experimental cross sections (Jones 1986) reported

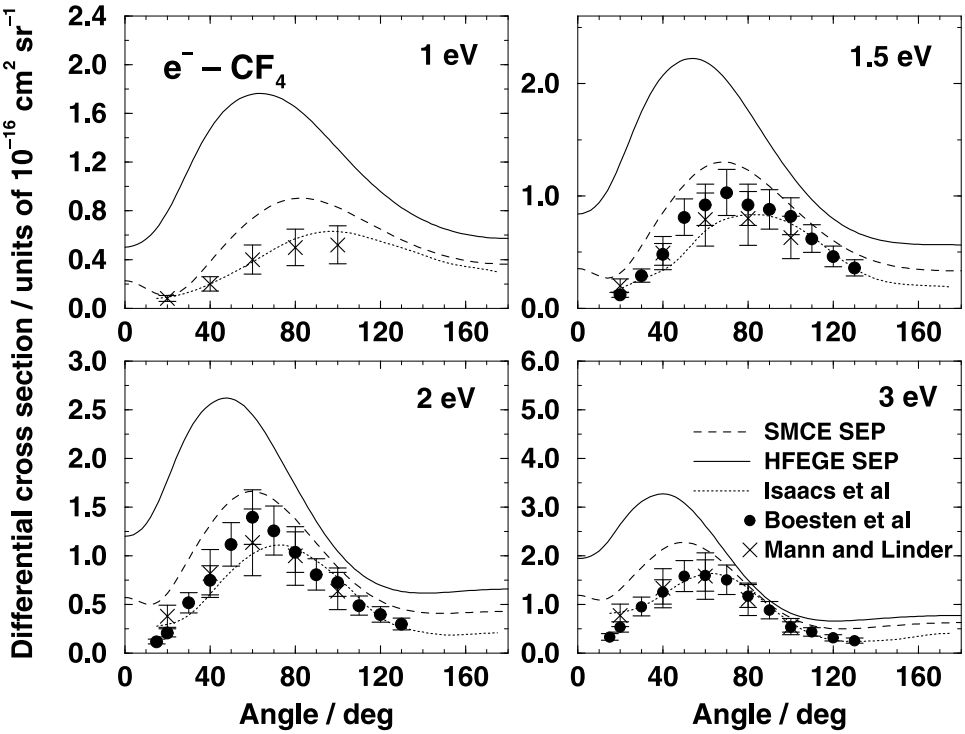

Figure 6. Computed and measured elastic DCS for electron–CF_4 at lower collision energies. The curves and symbols are labelled as in figure 5.

the presence of two low-energy peaks at 1.2 and 7.5 eV. The latter feature further appeared to be located on the low-energy side of a broad maximum. The electron transmission experiments of Burrow *et al* (1982) observed a peak at 0.94 eV and attributed it to a shape resonance of T_2 symmetry due to electron capture into a triply degenerate carbon chlorine antibonding orbital (σ^* orbital). This result was only qualitatively confirmed by the model calculations of Tossell and Davenport (1984), who found the resonance at 1.4 eV, before a broad maximum associated with a weaker and broader E resonance around 9 eV. In this study, our calculations suggest a further possible low-energy resonance of A_1 symmetry very close to threshold, confirm the T_2 resonance and further surmise a broad resonance of E symmetry around 9 eV. On the whole, the magnitude of our computed cross sections agree well with those from the experiments. It is interesting to note that electron scattering cross sections for both systems indicate the presence of low-energy Ramsauer–Townsend minima, features that we shall see are absent in the case of positron scattering.

A further assessment of the quality of the present scattering calculations via non-empirical model potentials could be had by comparing out results with the experimental angular distributions at selected energy values (Boesten *et al* 1992). The comparison for the case of CF_4 is shown in figures 5 and 6 and the energy values cover the resonance region (at 5 and 8 eV) in the upper panels of figure 5 and two higher energy values (10 and 15 eV) in the lower two panels of the same figure. The computed differential cross sections (DCS) in the very low-energy region are all shown in figure 6 and are compared both with experiments (Boesten *et al* 1992, Mann and Linder 1991) and with the latest calculations (Isaacs *et al* 1998). Our computed DCS values agree remarkably well with experiments at the higher energies and

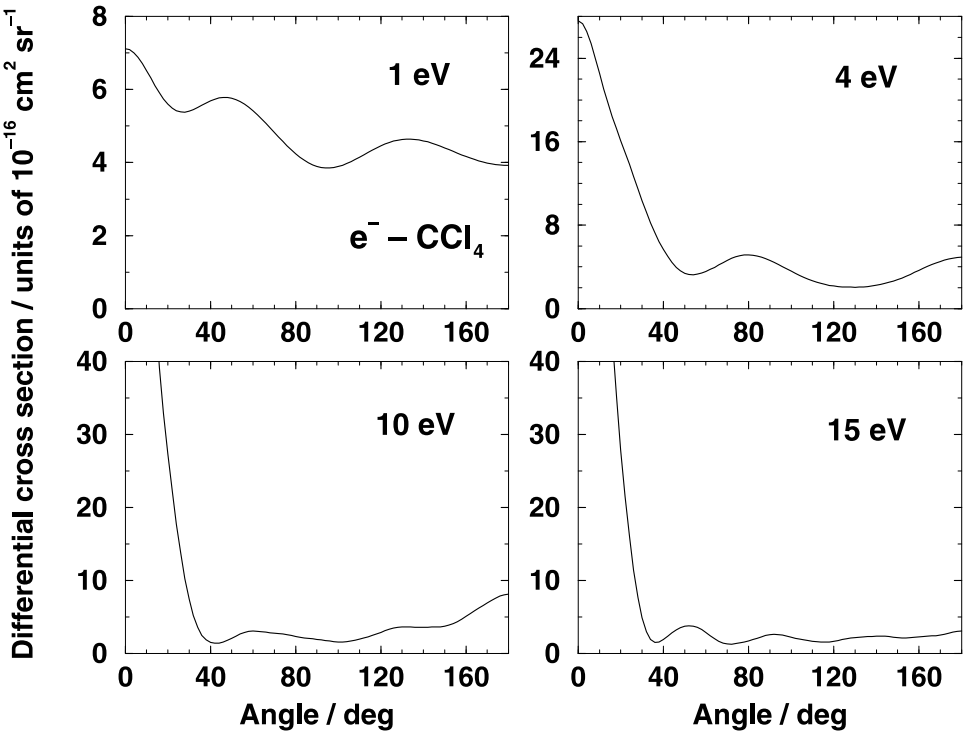

Figure 7. Computed elastic differential cross sections for electron scattering from CCl_4 at four different values of collision energy. The full curves and the broken curves have the same meaning as for CF_4.

also follow the measured data closely at lower energies. The small-angle region at 5 eV shows the largest discrepancy between computed and measured DCS, which is possibly an indication of the quantitative inadequacy of our V_{ecp} model for such scattering features that are dominated by long-range interaction. No comparable data exist from measurements for the CCl_4 molecules, but we have carried out similar calculations for that system in order to see whether further information on the collision process could be gleaned for it. The computed elastic (rotationally summed) DCS are reported in figure 7. The chosen collision energies correspond to the two low-energy peaks in the cross sections of figure 3 (upper two panels) and to two different energies in the region of the broad maximum (lower two panels).

One clearly sees that, away from the possible existence of marked resonant features, the angular distributions remain predominantly forward-peaked and therefore the DCS values below 40° are much larger then in the case of CF_4. At the lowest collision energy, on the other hand, the angular distribution changes completely and the presence of a minimum region in the integral cross section is reflected in a rather oscillatory dependence on the scattering angle of the corresponding DCS (upper left-hand panel in the figure).

4. Positron scattering cross sections

As mentioned in the introduction, the different features of the positron–molecule interaction potential are expected to correspondingly generate marked differences in the behaviour of the

cross sections even at the level of the simpler elastic scattering. The corresponding comparative measurements on CF_4 targets (Sueoka *et al* 1998) have recently shown that in the low-energy scattering region, where elastic positron collisions are expected to dominate, the e^+–CF_4 system is very different from the e^-–CF_4 case: cross sections are much smaller for the former system and do not show at all the marked decrease with energy seen for the electron–CF_4 scattering.

One of the questions which is still open, however, is how to realistically describe, just in that energy regime, the multicentre correlation forces between the impinging positron and the bound target electrons. In the previous section that described our methods, we have presented three different approaches to modelling such correlation forces for a positron and have seen, in figure 1, that they lead to very different strengths for the corresponding potentials in the short-range regions.

The computed cross sections are presented in figure 8, where we compare the experiments of Sueoka *et al* (1998) with three sets of calculations. The actual numerical results are reported, for a selected range of energies, in table 2. The strongest potential in the inner region was shown in figure 1 to be the V_{pcp} potential. The corresponding total cross sections in figure 8 (broken curve) are the largest at the lower collision energies, as expected, but remain lower than experiments above 2 eV. They exhibit, however, general agreement with the energy dependence of the experimental cross sections. The weaker V_{ecp} potential, on the other hand, seems to produce cross sections which are definitely too large above 1 eV collision energy: the dominant

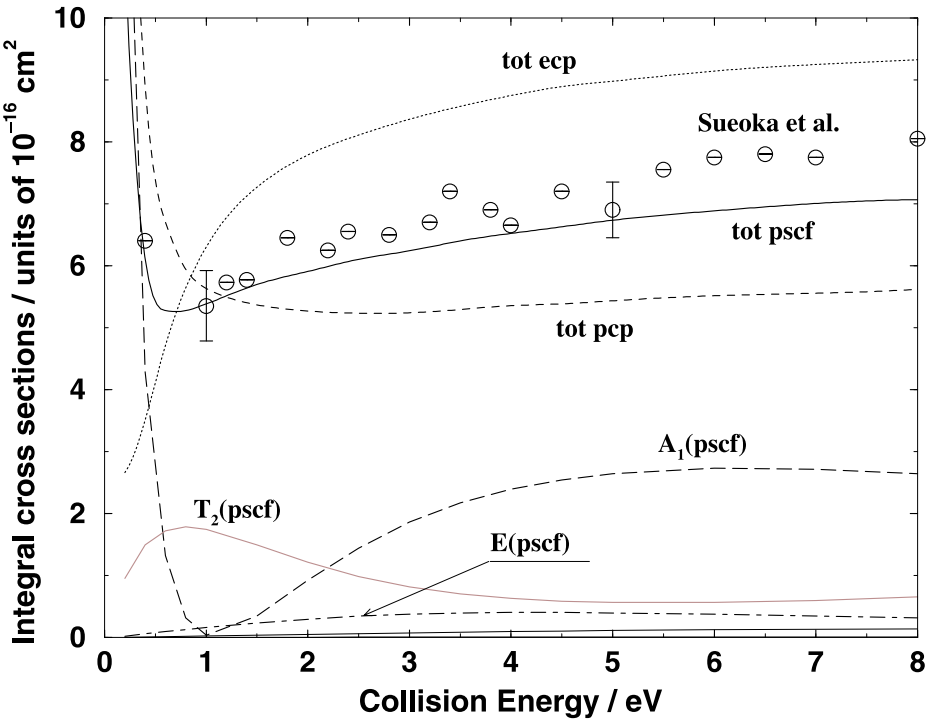

Figure 8. Computed and measured integral cross sections for positron scattering from CF_4. The open circles are the experiments from Sueoka *et al* (1998). The present calculations refer to our three different choices of correlation–polarization potentials. Full curve, using the V_{pscf}; broken curve, using the V_{pcp} potential; dotted curve, using the V_{ecp} interaction. The partial cross sections for the different symmetry contributions are shown for the V_{pscf} case only.

Table 2. Computed total integral elastic cross sections for positron scattering from CF_4 and CCl_4. Energies in eV and cross sections in $Å^2$ (calculations with V_{pscf}).

E (eV)	$\sigma_{tot}(CF_4)$	σ_{tot} (CCl_4)
0.4	6.10	161.21
0.8	5.28	101.72
1.0	5.38	87.88
2.0	5.91	56.14
3.0	6.24	43.45
4.0	6.52	36.29
5.0	6.73	31.74
6.0	6.88	28.56
7.0	7.00	26.31
8.0	7.06	24.48

repulsive interaction with the large, off-centre nuclei is not offset by the modelling of the attractive forces provided by the V_{ecp} interaction.

The simple V_{pscf}, on the other hand, is seen to be somewhat in between the previous models and to produce the short-range attraction due to the electron–positron correlation forces that is similar to that from V_{pcp}, while being weaker than the latter potential in the intermediate radial range. A consequence of these features, therefore, is that the cross sections are now in remarkable agreement with the measured data, as shown by the full curve of figure 8. The partial contributions of the dominant symmetries are also shown in the figure, where we see that the T_2 component is larger then the E component but that the totally symmetric contribution from the A_1 IR clearly controls the overall shape of the cross sections.

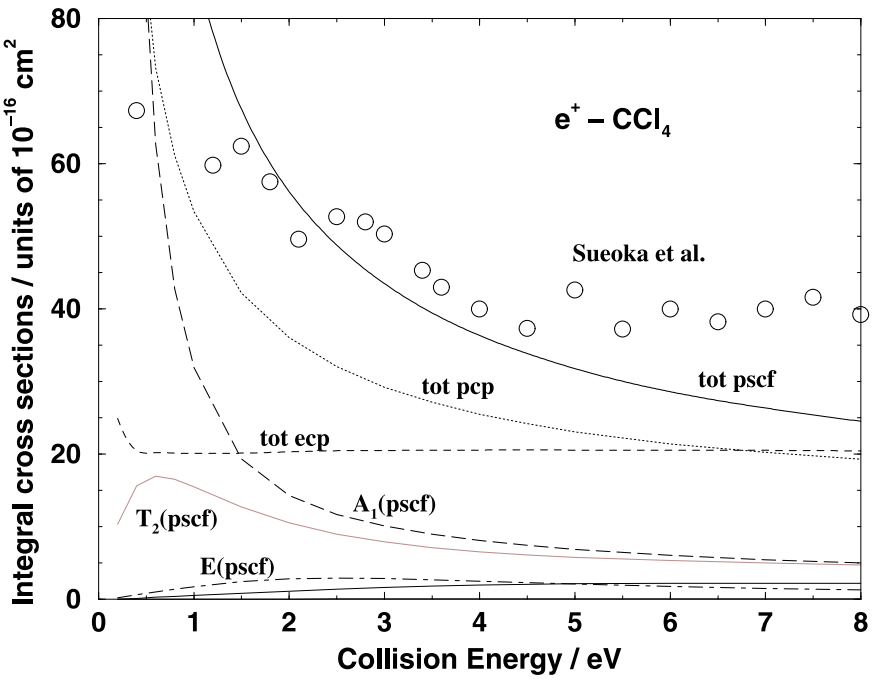

Figure 9. Same as figure 8 but for the CCl_4 target molecule. The open circles refer to the experiments from Sueoka *et al* (1998).

The situation is somewhat different in the case of CCl_4, for which we report comparison with experiments in figure 9. The actual numerical results are reported, for a selected range of energies, in table 2. The measured data are from Kimura *et al* (1999), while the calculations have been carried out with all three model correlation–polarization potentials discussed before.

When comparing the experimental data between electron and positron scattering from CCl_4 (Kimura *et al* 1999) it was pointed out that the positron integral cross sections showed a slowly decreasing trend at energies higher than 5–6 eV and dropped much faster below this region, thus decreasing with increasing energy at all the measured energies. The cross sections further showed a marked increase as the energy decreased below 5 eV, becoming very large at the lowest energies, as one can see from the data of figure 9.

The present calculations follow this low-energy behaviour, at least up to about 7 eV, where the threshold for positronium formation is reached and therefore the additional channels related to it open up in the experiments, but are absent in our treatment. As in the case of the CF_4 target, the V_{pscf} polarization-correlation potential model produces the best agreement with experiments: from figure 1 we see that indeed the latter potential is the strongest at the shortest distances and therefore is likely to be responsible for the fact that the corresponding total cross sections obtained with it (full curve in figure 9) are the largest at all energies.

As in the previous case, the scattering at the lower energies is dominated by the spherically symmetric component, A_1, the one which contains the long-range effect of the spherical polarizability employed to generate V_{pol}. In fact, the α_0 value for CCl_4 is more than three times larger than that for CF_4, hence when comparing the integral cross sections of figures 8 and 9, we see that those for CCl_4 are more than ten times larger then those for CF_4 at the low energies below 2 eV. This feature is in keeping with the general understanding that low-energy cross sections are largely controlled by the dipole polarizabilities of the molecular targets, especially when no exchange interaction contributes to the scattering.

The A_1 symmetry contribution to the total cross section is found here, at all the examined energies, to be the largest (see the three leading components plotted in figure 9 for the PSCF cross sections) for the CCl_4 target, thus suggesting that no minimum feature can appear in the final integral cross section. This result differs from that for the CF_4 system, where we clearly saw in figure 8 the appearance of a broad minimum in the cross sections, possibly due to the interplay between V_{pscf} and the static interaction.

In order to extend the comparison between e^+ and e^- scattering to the angular distributions, we report in figure 10 those for positron collisions, choosing two energy values for each molecule: the DCS at 1 eV, i.e. at very low collision energy, and the behaviour of the angular distribution at 4 eV, where the integral cross sections for both systems show a slower dependence on energy.

Both molecular targets clearly exhibit dominance of the forward scattering region, as expected by potentials which contain a large attractive component which ultimately dominates over the localized, short-range repulsion of the nuclear cusps distributed over the molecular volume. On the other hand, we see clear differences between CCl_4 and CF_4. The former molecule shows very strong forward scattering which rapidly decays to much smaller intensities beyond 40°, while the latter target exhibits less intense forward scattering and contributions from the large-angle regions play a more important role than in the case of CCl_4. The latter molecule, of course, yields angular intensities which are much larger than the former, another sign of the role of the differences in the polarizability values between the two targets.

As the previous model cross sections for electron scattering processes have shown, similar model calculations with positron projectiles (among the first to be carried out on polyatomic, multielectron systems such as the halogenated hydrocarbons) have exhibited quite good agreement with existing experiments and have been shown to be capable of yielding fairly

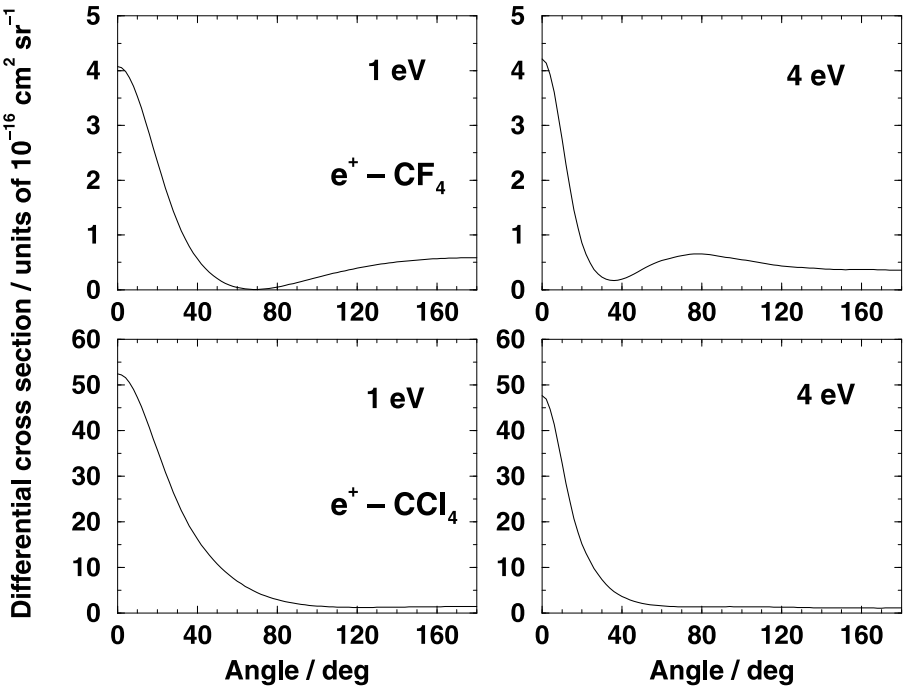

Figure 10. Computed elastic angular distributions, at two different collision energies, for positron scattering from CF_4 targets (upper panels) and from CCl_4 targets (lower panels).

realistic representation of the scattering process.

5. Conclusions

The main aims of the present calculations have been at least twofold: (a) we wanted to test the level of realistic representation of the elastic cross sections, integral and differential, which could be obtained through the use of non-empirical, parameter-free model interaction forces for multielectron polyatomic targets and (b) we also wanted to compare the outcomes from the evaluation of various scattering attributes for the same molecular targets with different projectiles such as electrons and positrons.

The chosen systems were both of T_d symmetry, had some experimental data available for comparison with calculations and had also been analysed by different theoretical and computational methods, thereby allowing the testing of our approach here which we mentioned above. On both counts we feel that the present results show that our choice of potential modelling is fairly realistic and can be used to obtain semiquantitative agreement, especially away from the threshold energy regions. Furthermore, the use of Volterra-type integral equations, of density-functional-based exchange and dynamical correlation effects and of single-centre expansion approach with exact static interactions and quantum, coupled scattering equations is seen to greatly reduce the computational efforts to only a few minutes per energy at each IR considered. These values have been compared with complex Kohn variational calculations which are orders of magnitude more intensive computationally and would be hard put to carry out exact SEP calculations for an all-electron target the size of CCl_4.

Several approximations, on the other hand, have been used here for electron and positron

scattering and their influence on the final comparison is not very easy to assess. First, we employ the FN approach at energies where vibrational and rotational channels are likely to contribute. Then we remove the non-locality of the exchange interaction and we replace electron–electron and electron–positron correlation forces with density-functional models. Lastly, we expand wavefunctions and potentials around the complex centre of mass, thereby having to assess convergence levels before carrying out the scattering calculations.

Although each item of the above list of shortcomings has been analysed by us over the years, their global effect can only be checked against existing measurements. The fact that such a check turns out to be fairly successful in the present case allows us to consider with some confidence further extensions of the method to inelastic channels involving molecular excitations. Such work is currently in progress in our group and will be reported elsewhere.

Acknowledgments

The financial support of the Italian National Research Council (CNR), of the Italian Ministry for University and Research (MURST) and the Supercomputing Center CASPUR is gratefully acknowledged. One of us (RC) further thanks the Supercomputing Consortium of CASPUR for the granting of a research training grant during which this work was completed.

References

Armour E A G 1989 *Comment. At. Mol. Phys.* **22** 173
Armour E A G and Baker D J 1987 *J. Phys. B: At. Mol. Phys.* **20** 6105
Arponen J and Pajanne E 1979 *Ann. Phys., NY* **121** 343
Bettega M H F, Ferreira L G and Lima M A P 1993 *Phys. Rev.* A **47** 1111
Boesten L, Tanaka H, Kobayashi A, Dillon M A and Kimura M 1992 *J. Phys. B: At. Mol. Opt. Phys.* **25** 1607
Boronski E and Nieminen R M 1986 *Phys. Rev.* B **34** 3820
Buckingham A D 1967 *Adv. Chem. Phys* **12** 107
Burrow P D, Modelli A, Chiu N S and Jordan K D 1982 *J. Chem. Phys.* **77** 1699
Christophorou L G, Olthoff J K and Rao M V V W 1996 *J. Chem. Phys. Ref. Data* **25** 1341
Dalgarno A and Lewis J T 1956 *Proc. Phys. Soc.* A **69** 57
Gianturco F A, De Fazio D, Rodriguez-Ruiz J A 1994a *Hyperfine Interact.* **89** 281
Gianturco F A and Jain A 1986 *Phys. Rep.* **143** 347
Gianturco F A, Jain A and Pantano L 1983 *J. Phys. B: At. Mol. Phys.* **16** 571
Gianturco F A and Lucchese R R 1996 *J. Phys. B: At. Mol. Opt. Phys.* **29** 3955
Gianturco F A, Lucchese R R and Sanna N 1994b *J. Chem. Phys.* **100** 6464
——1996 *J. Chem. Phys.* **104** 6482
Gianturco F A, Rodriguez-Ruiz J A and Jain A K 1993 *Phys. Rev.* A **48** 4321
Gianturco F A and Scialla S 1987a *J. Phys. B: At. Mol. Opt. Phys.* **20** 3171
——1987b *J. Chem. Phys.* **87** 6468
——1987c *Phys. Rev.* A **36** 557
Griffith T C 1979 *Adv. At. Mol. Phys.* **15** 135
Hara S 1967 *J. Phys. Soc. Japan* **22** 710
Humbertson J W and Armour E A G (ed) 1988 *Atomic Physics with Positrons* (New York: Plenum)
Huo W M and Gianturco F A (ed) 1995 *Computational Methods for Electron–Molecule Collisions* (New York: Plenum)
Isaacs W A, Mc Curdy C W and Rescigno T N 1998 *Phys. Rev.* A **58** 1
Itikawa I 1997 *Int. Rev. Phys. Chem.* **16** 155
Jain A and Gianturco F A 1991 *J. Phys. B: At. Mol. Opt. Phys.* **24** 2387
Jones R K 1986 *J. Chem. Phys.* **84** 813
Kimura M, Sueoka O, Hamada A and Itikawa Y 1999 *Adv. Chem. Phys.* at press
Mann A and Linder F 1991 *J. Phys. B: At. Mol. Opt. Phys.* **25** 533
Massey H S W 1932 *Can. J. Phys.* **60** 461

Mc Alinden M, Kernogham A A and Walters M R J (ed) 1994 *Positron Interactions with Atoms Molecules and Clusters* (Amsterdam: Balzer)
Miller K J 1990 *J. Am. Chem. Soc.* **112** 8533
Natalense A P P, Bettega M H F, Ferreira L G and Lima M A P 1995 *Phys. Rev.* A **52** R1
Parr R G and Yang W 1989 *Density Functional Theory of Atoms and Molecules* (Oxford: Oxford University Press)
Pritsch M J *et al* 1995 *Gaussian 94* Revision B.2 (Pittsburg, PA: Gaussian)
Rescigno T N and Orel A E 1981 *Phys. Rev.* A **24** 1267
——1982 *Phys. Rev.* A **25** 2402
Riley M E and Truhlar D G 1975 *J. Chem. Phys.* **63** 2182
Sams W N and Kouri D J 1969 *J. Chem. Phys.* **51** 4809
Sueoka O, Takaki H, Hamada A, Sato M and Kimura M 1998 *Chem. Phys. Lett.* **288** 124
Tossel J A and Davenport J W 1984 *J. Chem. Phys.* **80** 813
Weast R C and Salby S M 1966 *Handbook of Chemistry and Physics* (Boca Raton, FL: Chemical Rubber Company)